Title	Simultaneous assimilation of surface drifter data, satellite and in situ observations for improved estimates of meso-scale variability in the Kuroshio Extension Region
Author(s)	Nishina, Kei; Ishikawa, Yoichi; Awaji, Toshiyuki
Citation	Journal of Oceanography (2013), 69(2): 175-190
Issue Date	2013-04
URL	http://hdl.handle.net/2433/173123
Right	The final publication is available at www.springerlink.com
Type	Journal Article
Textversion	author

Simultaneous assimilation of surface drifter data, satellite and in-situ observations for improved estimates of meso-scale variability in the Kuroshio Extension Region

Kei Nishina · Yoichi Ishikawa · Toshiyuki Awaji

Abstract In order to better estimate meso-scale variabilities in the energetic Kuroshio Extension (KE) region, simultaneous assimilation of drifter-derived velocity data together with satellite and in-situ hydrographic data is attempted by using a high resolution 4-dimensional variational data assimilation (4D-VAR) system. Our experimental results, both with and without assimilation of drifter data (Exp. Drf and Exp. Ref, respectively) for the period during Aug-Oct 2005, show that the reproduced fields in Exp. Drf better reflect the observed meso-scale features such as the KE meandering jet and associated eddies. The adjoint sensitivity analysis indicates that our 4D-VAR system has the ability to provide a more realistic timeseries of the meandering jet structures that play a key role in the intergyre exchange between the subtropical and subarctic gyres in the North Pacific. In addition, the observed information from the surface drifters works to improve the subsurface structure. These results illustrate the advantage of our 4D-VAR simultaneous assimilation with the addition of drifter-derived surface velocity information.

K. Nishina · T. Awaji
Department of Geophysics, Graduate school of Science, Kyoto University, Kitashirakawa-oiwake-cho, Sakyo-ku, Kyoto 606-8502, Japan
Tel.: +81-75-753-3923
Fax: +81-75-753-3928
E-mail: nishinak@kugi.kyoto-u.ac.jp

Y. Ishikawa
Data Research Center for Marine-Earth Sciences, Japan Agency for Marine-Earth Science and Technology, 3173-25 Showa-machi, Kanazawa-ku, Kanagawa 236-0001, Japan
E-mail: ishikaway@jamstec.go.jp

1 Introduction

The energetic meso-scale variability in the Kuroshio Extension (KE) region plays a key role in the meridional heat and material transport in the North Pacific Ocean (e.g. Talley, 2003). In fact, previous studies reported that the Kuroshio, which supplies the Kuroshio Extension water, transports a huge amount of heat of up to 2.0 PetaWatt (PW = 10^{15} Watt) from subtropical to midlatitude regions (see Fig. 1). After the Kuroshio separates from the coast of Japan, a significant amount of heat is carried to the subarctic region across the meandering KE jet via the Kuroshio-Oyashio mixed water region (MWR) (Yasuda, 2003). Such a significant "cross-frontal" transport is reported to be associated with vigorous meso-scale variability (such as finite-amplitude meanders evolving into detached eddies and streamers) by both field and theoretical studies (e.g. Bower, 1991; Flierl, 1981). Thus the accurate monitoring and quantitative evaluation of cross-frontal transports in the KE region is relevant to understand climate change, material circulation, and oceanic ecosystems in the North Pacific Ocean.

Satellite observations have the advantage of wide coverage for oceanic processes in near-real-time. In fact, satellite-derived sea surface height (SSH) data are capable of providing dynamical information including subsurface structure, and thereby strengthen our understanding of variations in the KE and the behavior of eddies (e.g. Ebuchi and Hanawa, 2000; Qiu and Chen, 2005; Qiu et al., 2007). However, the spatio-temporal coverage of current SSH observations are still not enough to describe the sequence of eddy detachment or streamers (Kawamura et al., 1986; Sugimoto et al., 1992). In contrast, high-resolution satellite sea surface temperature (SST) observations are better able to capture prominent features on short-timescales, although they are unable to describe the dynamic behavior and subsurface structure of KE and eddies. Most recently, both satellite synthetic aperture radar (SAR; e.g. Chapron et al., 2005; Romeiser and Runge, 2007; Johannessen et al., 2008; Romeiser et al., 2010) and optical techniques (Matthews, 2005; Matthews and Awaji, 2010) provide synoptic scale surface currents at between 100 m and 1 km resolution. These new-generation satellite observations combined with SSH and SST are expected to improve our knowledge of meso-scale variabilities.

On the other hand, current-state-of-the-art ocean general circulation models (OGCM) are likely to offer high spatio-temporal resolution as far as computational capacity allows and, in fact, give some of important insights into meso-scale variabilities in the KE region (e.g. Mitsudera et al., 2004; Ishikawa and Ishizaki, 2009). However, the current performance of OGCMs is still not sufficiently advanced to reproduce the details of the KE region and to evaluate cross-frontal transport associated with meso-scale variability due to their biases in reproducing KE axis and the eddy kinetic energy (EKE) distribution in the KE region (e.g. Hurlburt et al., 1996; Kelly et al., 2007).

Within this background, data assimilation methods have recently focused on obtaining an optimal synthesis of observational data and model results for better descriptions of the ocean state. In particular, the 4-dimensional varia-

tional (4D-VAR) assimilation method has become highly attractive since it can provide a dynamically self-consistent dataset that best fits a variety of observations. Using the 4D-VAR method and state-of-the-art OGCMs, Masuda et al. (2003, 2006) recently provided a realistic large-scale ocean reanalysis dataset which was capable of assessing the dynamic state of large-scale ocean circulation and was relevant to the diagnosis of the transport pathways of heat and watermasses. However, due to the coarse spatial resolutions of their OGCM (roughly 1°), their system is not suited to define meso-scale variability. When attempting to reproduce processes associated with meso-scale variability, such as eddy activities and meandering jets, a finer resolution OGCM is required (e.g. Fukumori and Wunsch, 1991). Although Usui et al. (2008a,b) have shown the capability of representing realistic features of meso-scale variabilities south of Japan, high sensitivity with finer resolution data assimilation is still one of the toughest challenges.

Most recently, Ishikawa et al. (2009) developed a 4D-VAR data assimilation system to better describe the meso-scale variability taking place in the KE region by assimilation of satellite and in-situ hydrological observations into a high resolution OGCM. They reported that meso-scale features associated with frontal structures and eddies were well defined and biases in the KE meander pattern inherent in non-assimilated calculations were largely suppressed in the assimilation results. However, important aspects of meso-scale features associated with frontal jets and eddies are still missing from their results. One of the reasons for this is the lack of observational data. Since velocity measurements likely provide essential information of prominent frontal structures associated with meso-scale variabilities, inclusion of such data should lead to more realistic model results.

In this paper, we perform a simultaneous assimilation of both drifter-derived velocity data and satellite and in-situ hydrographic data into the high-resolution 4D-VAR data assimilation system (Ishikawa et al., 2009), and investigate the impact of improved estimates of meso-scale variability in the KE region. Surface drifters are often used for surface velocity observations because of their wide coverage, autonomous observational capacity and good cost performance. Absolute velocity data obtained from surface drifters are very effective for the diagnosis of ocean surface circulation (e.g. Niiler et al., 2003). In fact, previous studies showed the potential of Lagrangian data to better estimate ocean states by a data assimilation system (e.g. Kamachi and O'Brien, 1995; Ide et al., 2002; Lin et al., 2007). Thus, surface drifter data are expected to provide unique information capable of improving the analysis field even though they provide irregular spatial coverage. In future, we anticipate that surface current data derived on more synoptic scales will become available from SAR, InSAR (Interferometric Synthetic Aperture Radar) and optical techniques. In the light of this new data possibility, the present paper can be viewed as a first step toward a more integrated approach to the inclusion of ocean surface current in assimilation studies.

The outline of this paper is as follows. In section 2, we explain the pre-processing of surface drifter data to obtain velocity data. In section 3, the

configuration of the data assimilation system and the settings used in the assimilation experiment are described. In section 4, results of the assimilation experiment are validated by comparison with assimilated and independent observational data. The effectiveness of drifter data assimilation is examined in section 5, and results are summarized in section 6.

2 Drifter Data

2.1 Surface Drifter Data

In general, surface drifters comprise a surface float and a drogue centered at around 15 m depth (e.g. Niiler et al., 1995). Since long-lived drifters often lose drogues, Pazan and Niiler (2001) recently proposed an approach to obtain the near-surface velocity from undrogued drifters. These drifter data are assembled, then quality-controlled and interpolated to a 6-hourly trajectory by using a kriging technique (Hansen and Poulain, 1996) at the Global Drifter Center at the Atlantic Oceanographic and Meteorological Laboratory (AOML). The 6-hourly post-processing data are distributed by the Marine Environmental Data Service (MEDS) in Canada.

2.2 Preprocessing

Some sophisticated assimilation methods utilizing drifter-derived Lagrangian information have been proposed in previous studies (e.g. Kamachi and O'Brien, 1995; Ide et al., 2002) and have indicated their superiority to the simple "pseudo-Lagrangian" method (the use of Lagrangian instruments as moving current meters) mainly due to their inclusion of the Lagrangian nature of the observations. On the other hand, Nodet (2006) reported that a good performance of the "pseudo-Lagrangian" method for the case of short-term sampling such as surface drifters, although his sophisticated method has advantages for the case of long-term sampling and large observational errors. Taking into account their results, we adopt the "pseudo-Lagrangian" method in this study. After removing trajectory data with errors beyond 10 km (corresponding to 0.05 m s^{-1} for velocity), we estimate velocity using the centered finite differences method and the wind-slip correction method (Pazan and Niiler, 2001), using the National Centers for Environmental Prediction (NCEP) / the National Center for Atmospheric Research (NCAR) reanalysis wind (Kalnay et al., 1996).

These 6 hourly wind-slip-corrected data are smoothed by the "curvature compensation" technique (Niiler et al., 2003) designed for retaining salient dynamic features such as eddies and meanders, which are suppressed by a simple along track averaging of trajectory data. When making daily averaged velocity data after removal of tidal and inertial motions, we use two local inertial periods as the half width of the filter, but use 24 hours instead of the

local inertial period in regions where local inertial period is shorter than 24 hours.

2.3 The Experimental Period

In this study, comparative experiments both with and without the assimilation of drifter data (hereafter Exp. Drf and Exp. Ref) are performed to clarify the impact of drifter data on the reproduction of meso-scale variabilities. In doing so, we focus on the period during Aug-Oct 2005 when satellite observations indicate vigorous meso-scale variabilities and a relatively large number of drifters were observed in the KE region (more than 10 drifters in the upstream KE region). Ishikawa et al. (2009) indicates that the assimilation period should be at most 1 month for optimum calculation, so that we divide our experimental period into three subsets: Period 1 (2005/7/29   8/25), Period 2 (2005/8/26   9/22), Period 3 (2005/9/23   10/21). A more detailed discussion of the assimilation period can be found in 3.1.3.

The number of daily dataset (longitude, latitude, zonal and meridional velocity) available are 370 (drogued) and 1050 (undrogued) in Period 1, 621 and 1264 in Period 2, and 497 and 1357 in Period 3, respectively. Figure 2 shows the spatial distribution of preprocessed daily absolute velocity at each drifter position for each Period and demonstrates that the drifter-derived velocity field well reflects the observed features of the energetic KE including its recirculation and pinched-off eddies. The data shows that approximately 15% of the daily velocities are faster than 0.5 m s^{-1}.

3 Experimental Design

3.1 The Data Assimilation System

For more details of the system, refer to Ishikawa et al. (2009).

3.1.1 Numerical Model

The numerical model used in this study is the OGCM developed at Kyoto University (e.g. Toyoda et al., 2004; Nakamura et al., 2006), which employs the hybrid $\sigma - z$ vertical coordinate to better simulate free surface motion of the ocean. To further enhance the representation of the upper ocean circulation, this model adopts some sophisticated parameterizations such as the Takano-Onishi scheme for the momentum equation (Ishizaki and Motoi, 1999), the turbulence closure scheme for the mixed layer parameterization (Noh and Kim, 1999; Noh, 2005), the 3rd order scheme (Hasumi, 2000) based on QUICK-EST (Leonard, 1979) for vertical advection and UTOPIA (Leonard et al., 1993) for horizontal advection, and the isopycnal mixing scheme (Gent and McWilliams, 1990; Griffies, 1998). The model basin covers the northwestern North Pacific which involves the Sea of Japan and other marginal seas

$(125 - 165°E, 25 - 50°N$, see Fig. 2). The horizontal resolution is $1/6°$ and $1/8°$ in longitude and latitude, respectively, with 78 vertical levels spaced from 4 m near the sea surface (in the rest state) to 500 m at the bottom.

For the surface boundary condition, the climatological monthly mean data derived from the ECMWF reanalysis dataset (Roske, 2001) are used. It should be noted that the surface heat flux is calculated by applying the bulk formulae (Ikeda, 1989) with the modeled SST. The initial and the boundary conditions are derived from the full North Pacific Ocean model calculation by using the nesting technique based on Oey and Chen (1992).

3.1.2 Observation Data

The assimilated elements (except for the drifter data) are satellite-derived SST and SSH data, and in-situ observations of temperature and salinity. In detail, the SST data are from the New Generation Sea Surface Temperature (NGSST) dataset produced at Tohoku University (`http://www.ocean.caos.tohoku.ac.jp/`) with a horizontal resolution of $1/20°$ and daily coverage. Since the resolution of this data set is finer than that of the numerical model, the data are averaged over each model grid and assimilated into the model based on the concept of super-observation (Lorenc, 1981). The SSH data are from the SSalto/Duacs gridded absolute dynamic topography, which is the sum of the merged sea level anomaly derived from available altimeter data and mean dynamic topography (Rio and Hernandez, 2004) provided by AVISO (`http://www.aviso.oceanobs.com/`) in time and space intervals of 3.5 days and nearly $1/3°$, respectively. The SSH data are interpolated onto the model grids for assimilation because the resolution of the model is finer than that of the data. The in-situ observation data are obtained from the global temperature-salinity profile program (GTSPP) provided by NOAA/NODC (`http://www.nodc.noaa.gov/GTSPP/`). For these data, both averaging and interpolation are used depending on the vertical resolutions of model and data.

3.1.3 Assimilation Scheme

In our 4D-VAR approach, optimized 4-dimensional datasets are sought by minimizing a cost function (e.g. Awaji et al., 2003), in which the initial condition of model variables is chosen as the control variable $\mathbf{c}$. The cost function is composed of the background and the observational term as

$$\mathbf{J} = (\mathbf{c} - \mathbf{c}_{\text{ini}})^{\text{T}} \mathbf{B}^{-1} (\mathbf{c} - \mathbf{c}_{\text{ini}}) + [\mathbf{H}(\mathbf{x}) - \mathbf{y}]^{\text{T}} \mathbf{R}^{-1} [\mathbf{H}(\mathbf{x}) - \mathbf{y}] \qquad (1)$$

where the notation follows Ide et al. (1997). The background error covariance matrix $\mathbf{B}$ is determined based on the spatio-temporal changes of the corresponding variables in some preliminary experiments. Here the observation error covariance matrix $\mathbf{R}$ is assumed to be diagonal for convenience. Further, the observational errors of SST and SSH are assumed to be horizontally uniform with values set at $1(C°)^2$ and $25(\text{cm})^2$, respectively. Also, the errors of

in-situ observations are assumed to be horizontally uniform and the vertical distribution of the magnitude is set as the level averaged diagonal component of the background error covariance multiplied by a factor of 0.01. This means that the observational data are assumed to be 10 times more accurate than the modeled data. Based on the preprocessing described in Sec. 2, the errors of drifter data are assumed to be uniform in value at 0.05^2 $(\text{m s}^{-1})^2$.

The operator $\mathbf{H}$ denotes an observation operator. For the SST and SSH data, the model outputs are averaged over 1 day and 3.5 days, respectively, to match the observational data. Similarly, for the in-situ profiling data of temperature and salinity, the model results are averaged over 1 day in time and $1°$ in the horizontal direction. For the surface drifter data, the model results are averaged over 1 day in time and over 4 grids adjacent to each observational point in the horizontal direction. In the vertical direction, model results from 0 m to 16 m depth are used for both the drogued and undrogued drifters.

The adjoint model, which transports the information of observational data backward in time, is formulated from the forward OGCM except for the mixed layer process. It should be noted that the vertical eddy diffusivity calculated in the forward model is used for the adjoint calculation. All parameters, such as horizontal viscosity and diffusivity are the same as in the forward run. In the adjoint calculation, the daily averaged results of the forward run are used by interpolation in time.

Ishikawa et al. (2009) carried out adjoint sensitivity experiments to seek a reasonable assimilation period for this high-resolution assimilation system. In these preliminary analyses, they showed that the adjoint model has the ability to propagate physically meaningful signals for up to approximately one month. Taking into account the results of the adjoint sensitivity experiments and the merit of a longer assimilation period with which a large number of observation data can be used to optimize the initial condition, they decided to adopt a 28-day assimilation period. Furthermore, they used a larger model region compared with the energetic KE region of our interest in order to suppress the effect of the boundary condition on the target region. Although a one-month assimilation window is somewhat longer than other oceanic high-resolution data assimilation systems (e.g. Moore et al., 2011; Yu et al., 2012), we believe this length is appropriate to our system by reason of the results of the preliminary investigation and the well thought-out design of the system. In fact, Ishikawa et al. (2009) show that their (our) system works well and produce a good dataset, which we expect to further improve in this study. Based on this previous study, we also use 28 days as the assimilation period of this experiment.

When minimizing the cost function, we use the POPULAR scheme (Fujii and Kamachi, 2003), which has the advantage of enabling the nondiagonal part of the background error covariance matrix to be readily utilized.

3.2 First Guess Field

We need to use a reasonable first guess field to steer the algorithm toward the most reasonable solution. For this purpose, we have made preliminary assimilation experiments to cover the 3-month period from May to July 2005 with no use of drifter data, and with the assimilation window set to one month. The first guess field in Period 1 is generated by a forecast calculation utilizing the preliminary experimental data on July 29th as an initial condition, followed by the comparative assimilation experiment in Period 1 for Exp. Ref and Exp. Drf. In Periods 2 and 3, first guess fields are calculated in a similar manner to those for Period 1 and the initial values in both cases are made by using the result from the previous Exp. Ref. An adjoint calculation for each Period is repeated until the cost function value reduces to a stable value (actually until the optimization process reaches 100 iterations). Although the result may not be an optimum solution due to the nonlinearity of vigorous meso-scale variabilities in the KE region, the reduction of the value of the cost function proves that the corrected field obtained in our assimilation system is expected to become closer to the 'true-state', as is shown below.

3.3 Independent Observation

To assess the validity of our assimilated result, we use the velocity data of the YoMaHa'07 (Lebedev et al., 2007, `http://apdrc.soest.hawaii.edu/projects/yomaha/`) dataset derived from Argo float trajectories provided by the Asia-Pacific Data-Research Center (APDRC) / the International Pacific Research Center (IPRC). This dataset contains estimates of both near-surface current velocities and values at the parking depth of the Argo float (hereafter called surface and deep velocities, respectively; the details of the estimation is expressed in Lebedev et al., 2007). Note that this dataset is not used for our assimilation experiment and hence is suitable for robust validation (we also use the assimilated elements for basic validation). In doing so, we use surface velocities whose errors are less than 0.05 m s^{-1} (about 20% of data are removed). As a result, approximately 400 surface velocity data points remain in the model region in each Period, more than half of which are distributed in the KE region $(140 - 156°\text{E}, 30 - 40°\text{N})$.

4 Results

To quantify the impact of the simultaneous assimilation of drifter data on the reproducibility of meso-scale variabilities, we calculate root mean square difference (RMSD: spatio-temporal mean) values between observations and analysis in both experiments. We define the improvement rate (hereafter IR) through the use of RMSD values as below

$$IR(i) = \frac{RMSD_{Ref}(i) - RMSD_{Drf}(i)}{RMSD_{Ref}(i)} \times 100, \qquad (2)$$

where i denotes the RMSD for some of physical variable. IR is the normalized difference of the RMSD values between both cases. We consider the value of IR(i) as a measure of increased hindcast skill by the addition of drifter data for a physical variable denoted by i. Table 1 shows the values of IR for each period and KE region, in which the various lines represent the IR for drifters, SST, SSH, vertical temperature profiles, vertical salinity profiles, and surface velocity data of YoMaHa'07 dataset, respectively. Table 1 indicates that surface circulations reproduced in the Exp. Drf case are in better agreement with the observed features than with those in Exp. Ref throughout all experimental Periods. This fact means that drifter data are successfully reflected in the assimilated results. The improvements are also visible in other assimilated elements, thereby implying that the addition of surface drifter data to our assimilation experiments works to improve not only the surface velocity field but other physical states of the KE region, including vertical structures. These superior results are due to the sophisticated 4D-Var assimilation capability of performing multivariate simultaneous assimilation (Fukumori and Wunsch, 1991; Stammer et al., 2002; Masuda et al., 2003). Furthermore, the improvement in the independent YoMaHa'07 dataset suggests that the analysis field in the Exp. Drf is a better fit to the 'true-state'.

Note that in Period 3, each IR value is negative except for the drifter data whose IR value remains positive. The reasons for this are considered as follows: The background field in Period 3 has relatively large errors which result in a decrease in the efficiency of the optimization process. In addition, a larger number of drifters observe the KE jet in Period 3 than in the other two periods. The effective weighting of the drifter data thus increases. Therefore, a strong correction of the meandering KE jet takes place under a condition of inefficient optimization due to the strong nonlinearity inherent in the energetic KE. As a result, the jet structure is well corrected (positive IR for drifter data), but the correction of the other regions is insufficient (negative IRs for the others). Moreover, in this strongly non-linear regime, the 4D-VAR technique inevitably provides a poorer quality of improvement to the background field. The fact that the number of drifter data in each period does not always have a close relation to the IR value suggests that better reproduction of the dynamic features of the background field is further important factor in improving the ocean state by making use of drifter information in a 4D-var data assimilation approach. If these considerations are correct, possible solutions may require a decrease of background errors by improving our numerical model or adopting a shorter assimilation window with modulation of the relative weights of the observations. A further investigation of this problem is for future work.

We focus on the meso-scale variabilities in Period 1 when the improvements resulting from the assimilation of drifter data are most significant. Figure 3 shows the mean SSH and SST fields averaged over Period 1 for both cases,

as well as the corresponding satellite-based objective map. Note that satellite SSH objective map provide reliable estimations on monthly timescales. Despite the small amount of drifter data relative to other observational data, considerable differences between the two cases are apparent in the roughly monthly-averaged fields, in which meso-scale structures appear. As expected by the value of IR for SSH in Table 1, the positions and strengths of meso-scale eddies in Exp. Drf become closer to the satellite SSH map than those in Exp. Ref (rectangular boxes with dashed black line). Figures 3d, e, f also suggest that some SST patterns in Exp. Drf are a better fit to the objective SST map than those in Exp. Ref in association with improvement of meso-scale structures (for example, the positive SST anomaly in the rectangular box A corresponds to an improved anticyclonic eddy). This means the SST distributions are corrected by improvements in the surface circulation field and the SSH field largely as a result of the corrections of the thermocline structures. More specific descriptions of improvements in Exp. Drf (for the regions around rectangular boxes A and B) are made in the following paragraphs using SSH snapshots and various data.

Figure 4 shows snapshots of an anticyclonic meso-scale eddy in Period 1 which is also visible in the monthly-averaged field (the rectangular box "A" in Fig. 3). Figures 4a and d show 3.5 daily satellite SSH objective maps with superimposed velocity vectors derived from the assimilated drifter data (black arrows) and the independent YoMaHa'07 dataset (dashed black arrows). Since the accuracy of a satellite objective map is not sufficient for the purpose of monitoring a time series of meso-scale structures in detail, we provide the objective map in black-and-white contours except in the area in which along-track data are available during the corresponding periods (color tone). Figures 4b, e and c, f show the reproduced SSH fields averaged over 3.5 days (color tone) with superimposed reproduced velocity vectors (in the same manner as Figs. 4a, d) in Exp. Ref and Exp. Drf, respectively. Consideration of the drifter observations and the satellite-derived SSH objective map (Fig. 3a, Figs. 4a and d) indicates the presence of an anticyclonic eddy near 149°E, 39°N. This anticyclonic eddy is also seen in the pattern of reproduced SSH fields of both cases. However, the feature of this pronounced anticyclonic eddy in Exp. Drf is closer to that of assimilated elements than in Exp. Ref. For example, the position of the eddy in Exp. Drf is corrected by approximately 1 degree both zonally and meridionally from that in Exp. Ref. Figures 3a and d and 4a indicate that satellite observations provide information on the location and strength of this eddy. However they seem insufficient to reproduce a realistic time-trajectory of the energetic meso-scale variability from the reproduction of Exp. Ref (Figs. 4b and e). It would appear that satellite data are utilized more effectively to reproduce this time-varying eddy following the simultaneous assimilation of drifter data. The agreement with independent YoMaHa'07 data is also improved to some extent in parallel with the improvement of the meso-scale eddy representation (see dashed arrows at 148°E, 38.5°N in Figs. 4d, e, f).

We next estimate the improvements of the KE jet in Period 1 (the rectangular box "B" in Fig. 3) by using Fig. 5 (in the same manner as Fig. 4). In Figs. 5a and d, drifter data indicate a strong northward velocity equivalent to the KE jet. However, corresponding velocity vectors in Exp. Ref (Figs. 5b and e) are not so strong due to a small westward meander of the KE jet. On the other hand, the axis of the KE jet in Exp. Drf are consistent with drifter data (Figs. 5c and f) in connection with the suppression of the unrealistic small meander in Exp. Ref. These corrections in Figs. 4 and 5 give us confidence in the superiority of our simultaneous assimilation using drifter data in estimating meso-scale variabilities. As indicated by the values of IR in Table 1, previously assimilated data are also used more efficiently and better reflect the reproduced field as a result of our simultaneous assimilation.

We confirm a further advantage of our 4D-VAR assimilation system by investigating Figs. 6 and 7. The satellite SSH and drifter velocities in Figs. 6a and d suggest that a cyclonic eddy is centered at 149°E, 39°N. The reproducibility of this eddy is comparable in the location of the eddy in these two cases. In terms of the strength of the eddy, the result of Exp. Drf is closer to the satellite SSH than that of Exp. Ref. Figures 7 show the temperature profiles at the positions indicated as blue plus symbols in Figs 6a, b, c. It is apparent that the vertical temperature profile of this cyclonic eddy in Exp. Drf is more consistent with the in-situ observations than that in Exp. Ref. The shallower thermocline in Exp. Drf means that the cyclonic circulation of the eddy in Exp. Drf is stronger than that in Exp. Ref. This change agrees well with the improvement in eddy strength inferred from SSH fields in Figs. 6. Therefore, we speculate that the improvements in the cyclonic eddy representation are not restricted to the sea surface but also extend down to intermediate layers. This means that information provided by the surface drifters works to correct the vertical structure via the numerical model in our 4D-VAR approach, thereby contributing to an improved representation of subsurface circulation. Note that the improvement of meso-scale variability is achieved in both vertical and horizontal domains by our multivariate simultaneous assimilation, thereby contributing to our understanding of cross-frontal heat and material transport and to watermass formation processes.

In this section, we demonstrate a better representation of meso-scale variabilities in Exp. Drf thanks to the addition of surface drifter data. Figures 4 and 6, however, indicate that the reproducibility of the detailed meso-scale structures can still be improved further. In particular, the amplitudes of eddies in our assimilated results look like they are smoothed in comparison to those in the satellite SSH objective maps (even for the reliable parts that are accompanied with along-track data and are consistent with surface drifters). This is because the results of our 4D-Var method depend on the model performance (especially on the horizontal resolution of the model in this case) and reflect its ability for optimization using the numerical model. Therefore, further improvements can be expected by upgrades of our numerical model. In addition, the SSH observations used as input to the assimilation system are themselves smoothed in comparison with the along-track data. It is also

important to make more efficient use of already assimilated elements such as the direct assimilation of along-track SSH data. These efforts toward a further improved synthetic dataset are necessary for the purpose of forecasting meso-scale variabilities or providing an accurate estimation of heat and material transports within a physically-consistent 4-dimensional oceanic dataset.

5 Effectiveness of Drifter Data Assimilation

In this section, an adjoint sensitivity analysis is carried out to identify the effectiveness of drifter data for the improvements of assimilation results. To initiate this approach, we use the first guess field of Period 1 as the background field of the analysis, since the correction derived from drifter data are clearer in this Period than in others. We aim to calculate the sensitivity to a velocity fluctuation (δu, δv) input to the crest of the KE jet (corresponding to the misfit between analysis and drifter data in the assimilation experiments), since the meandering of the jet stream is essential in the KE dynamics and tends to have a large misfit. Taking into account the fact that the zonal component dominates in the velocity field at the input area, we set $|\delta u|$ to be more than 10 times larger than $|\delta v|$. The sign of δu is set to be negative, which corresponds to the situation that the zonal velocity in the model is smaller than that derived from drifter data. Note that both δu and δv are input to a region of $1/3° \times 1/4°$ in the horizontal direction and 0 m to 16 m in the vertical direction ($2 \times 2 \times 5$ grids) during the last day of the background field (equal to the first day of the adjoint analysis). For simplicity, we focus on the behavior of adjoint signals in the top layer (hereafter called λ_u). In addition, an unequally-spaced color tone is used to represent the magnitude of λ_u. Specifically, a color represents a value range from $10^{x/2}$ to $10^{(x+1)/2}$ except for values around zero (see Figs. 8, 9). This scale is adequate to describe the time-evolution of λ_u from a relatively small input region as compared with the KE analysis region (the latter is more than 1000 times larger than the former).

Firstly, we explain the initial distribution of λ_u. Figure 8a shows both the distribution of λ_u around the input region and the background SSH field at the time tracked back to 1 day from the start of the initial input (hereafter called day -1). The structure of λ_u in Fig. 8 is thought to be formed by the dynamical adjustment to the input of δu and the background advection. The dynamical adjustment is mainly via geostrophic adjustment, which shows the existence of both positive and negative values in spite of the negative initial input. Note that the signal advected by the KE jet propagates westward, because the adjoint model transports information backward in time. Furthermore, there are some signals to the east of the input region in Fig. 8a, suggesting that gravity waves are also generated by the initial signal and thereby not only background circulation but waves contribute to the propagation of information.

Next, we examine the time series of λ_u shown in the panels of Fig. 9. The adjoint signals have a pronounced westward propagating tendency around the KE jet on day -1 as a result of advection in the sense of backward calcula-

tion. The edge of the λ_u distribution reaches 142°E on day -7. The speed of horizontal spread is estimated to be approximately coincident with the zonal velocity of the KE stream, whereas part of λ_u propagates across SSH isolines to the north and south recirculation gyres (surrounded by dashed black line in Fig. 9c). The across-isoline propagation of λ_u may be attributed mainly to two factors, (1) time variation of the background circulation field (stream lines are different from particle pathways in an unsteady state) and (2) processes of separation and capture of fluid parcels by a meandering jet (Cushman-Roisin, 1994). Therefore, the advection effect by the background circulation field plays a central role in maintaining signals within the recirculation gyres. On day -4 (Fig. 9b), positive and negative values appear alternately around the KE jet presumably due to the initial dynamical adjustment and wave effects. This wave-like structure affects the dipole pattern of λ_u within the recirculation gyres (Fig. 9c).

As time advances (in the sense of the backward calculation), λ_u on the KE jet is advected outside the KE region and partly separates out to the periphery of the jet. Thus the adjoint signals spread to the whole KE system overlying the recirculation gyres, crest and trough of the meandering jet (Fig. 9d; day -14). A similar situation in which signals are trapped is identified on day -21(Fig. 9e), in which the southern recirculation gyre captures over 40% of λ_u in the KE region (the dashed black square in Figs. 9d and e; from day -7 to day -21). Hence, a large amount of the signal remains in the KE region for approximately 2 weeks, although the signals become rather sparse in Fig. 9f (day -28). The decrease in signal strength seen in Fig. 9f is associated with wave radiation, diffusion, time variation of the background field and so on. Since the meandering stream and its associated recirculation gyres are core elements of the KE system, these facts underline our conclusion that assimilation of additional drifter data into the model by our 4D-Var approach works well in correcting the KE variation.

In addition to the horizontal propagation described above, we take a brief look at the vertical structure of the adjoint sensitivity in the zonal velocity and temperature field. For this purpose, we perform an additional adjoint sensitivity experiment in which the initial signal is input into a region with weak background circulation. The settings of this additional experiment are the same as the experiment described in previous paragraphs, except for the input region. We pay attention only to the state on day -1 for simplicity. Figure 10a is the same as Fig. 8, but for this additional experiment. Figure 10b is the same as Fig 10a, but for the distribution of the adjoint signals in the temperature field in the top layer. Figures 10a and b illustrate that the adjoint signals in the temperature field appear to be geostrophycally balanced with those in the velocity field. Also note that the earlier condition, in which the structure of λ_u in Fig. 8 is formed by the dynamical adjustment and the background advection, can be reconfirmed by the comparison of Fig. 8 and Fig. 10a. Figures 11a and b show the meridional sections of Figs. 10a and b with superimposed background temperature field. Figure 11a indicates that strong adjoint zonal velocity signals appear near the sea surface probably due

to the effect of initial input signals trapped into the summer shallow mixed layer. Below the mixed layer, the vertical distribution of the adjoint signals reflects the background temperature stratification. Although the intensity of the signals below the mixed layer is weak compared with the remaining initial input above the mixed layer, this vertical structure corresponding to the vertical modes is interesting in terms of physical oceanography. On the other hand, adjoint temperature signals reach the upper part of the thermocline (approximately 300m depth) with a considerable strength (approximately 10 % of the maximum). This feature of adjoint temperature signals is physically reasonable in terms of its ability to improve the structure of the thermocline in agreement with the correction of the surface velocity field. This consideration is also consistent with the improvements to the temperature profiles shown in Figs. 7, especially for the thermocline structures. Therefore, surface drifter data are able to improve the circulation field and temperature field at the same time through this vertical propagation within the 4D-Var method, a process which also satisfies the model dynamics and reflects the background stratification. After this adjustment to the initial input of velocity data, these structures propagate 3-dimensionally according to the model dynamics such as background advection and mode waves. More detailed discussions, such as detailed explanations of the vertical structures of adjoint signals, remain a challenge for the future.

6 Summary

We have performed a pair of advanced simultaneous assimilation experiments with (Exp. Drf) and without (Exp. Ref) drifter-derived velocity data using our high-resolution 4D-VAR data assimilation system, together with satellite and in-situ hydrographic data. We then compared the results for the period during Aug-Oct 2005 when satellite observations indicate vigorous meso-scale variabilities and a relatively large number of drifters were located in the KE region. This study can be viewed as a first step of multivariate simultaneous assimilation system including velocity data for when the better surface current fields provided by SAR/InSAR or optical methods become available.

Despite the small amount of drifter data relative to the satellite observations, considerable differences in the reproduced meso-scale features between Exp. Ref and Exp. Drf are found in monthly averaged SSH fields (Fig. 3), suggesting that the impact of drifter data assimilation on improving the reproduction of meso-scale variabilities observed in the KE region is important. The superiority of our simultaneous assimilation using drifter data is also confirmed by the fact that the RMSD values in the Exp. Drf case are smaller than those in the Exp. Ref case not only for the circulation field derived from surface drifter data and the independent YoMaHa'07 dataset but also the temperature-salinity field derived from satellite and in-situ data (Table 1). Particularly in the first assimilation period (Period 1), the agreement with observations is greatly improved (Table 1). Close examination of the repro-

duced meso-scale structures (anticyclonic and cyclonic eddies, and KE jet) in Period 1 shows that their features (location and strength) in Exp. Drf are more similar to the assimilated elements when compared with those in Exp. Ref (Figs. 4, 5, 6). Associated with the improvement in dynamic behavior of the KE system characterized by the meandering jet and its recirculation, the vertical structure of the cyclonic eddy is also better defined down to intermediate layers due to the dynamic correction from shallower layers generated by the sophisticated 4D-VAR approach coupled with the OGCM (Figs. 7).

Although surface drifters provide irregular spatial coverage and a small amount of information compared with satellite observations, their impact on improving assimilation results is significant. This fact indicates that simultaneous assimilation with the addition of synoptic surface current fields provided by SAR/InSAR or optical methods would dramatically improve our synthetic dataset, and hence that the next generation of experiments should be performed with this in mind.

The evaluation of cross-frontal heat and material transport, which is important in terms of inter-gyre exchange in the North Pacific, remains to be carried out, since this evaluation requires a dataset with longer period and broader coverage down to the subsurface layers. In this regard, the YoMaHa'07 dataset of subsurface velocity are promising. Nevertheless our study illustrates the superiority of the dataset obtained from the multivariate simultaneous assimilation with the addition of drifter data, and thereby underlies the usefulness of this approach for understanding the complicated meso-scale features in the KE region and in formulating the cross-frontal heat and material transports associated with meso-scale variabilities.

References

Awaji, T., S. Masuda, Y. Ishikawa, N. Sugiura, T. Toyoda, and T. Nakamura, 2003: State Estimation of the North Pacific Ocean by a Four Dimensional Variational Data Assimilation Experiment. *J. Oceanogr.*, **59**, 931–943.

Bower, A. S., 1991: A simple kinematic mechanism for mixing fluid parcels across a meandering jet. *J. Phys. Oceanogr.*, **21**, 173–180.

Chapron, B., F. Collard, and F. Ardhuin, 2005: Direct measurements of ocean surface velocity from space: Interpretation and validation. *J. Geophys. Res.*, **110**, C07 008, doi:10.1029/2004JC002809.

Cushman-Roisin, B., 1994: Introduction to geophysical fluid dynamics (second edition). *Prentice Hall College Div,*, 244.

Ebuchi, N. and K. Hanawa, 2000: Mesoscale Eddies Observed by TOLEX-ADCP and TOPEX/POSEIDON altimeter in the Kuroshio Recirculation Region South of Japan. *J. Oceanogr.*, **56**, 43–57.

Flierl, G. R., 1981: Particle motions in large amplitude wave fields. *Geophys. Astrophys. Fluid Dyn.*, **18**, 39–74.

Fujii, Y. and M. Kamachi, 2003: A Nonlinear Preconditioned Quasi-Newton Method Without Inversion of a First-Guess Covariance Matrix in Variational Analyses. *Tellus, Series-A*, **55**, 450–454.

Fukumori, I. and C. Wunsch, 1991: Efficient representation of North Atlantic hydrographic and chemical distribution. *Prog. Oceanogr.*, **27**, 111–195.

Gent, P. R. and J. C. McWilliams, 1990: Isopycnal mixing in the ocean circulation model. *J. Phys. Oceanogr.*, **20**, 150–155.

Griffies, S. M., 1998: The gent-mcwilliams skew flux. *J. Phys. Oceanogr.*, **28**, 831–841.

Hansen, D. V. and P. M. Poulain, 1996: Quality control and interpolations of WOCE-TOGA drifter data. *J. Atmos. Oceanic Technol.*, **13**, 900–909.

Hasumi, H., 2000: Ccsr ocean component model (coco) version 2.1. *CCSR Report*, **No. 13**, center for Climate System Research, U. of Tokyo.

Hurlburt, H. E., A. J. Wallcraft, W. J. Schmitz Jr., P. J. Hogan, and E. J. Metzger, 1996: Dynamics of the Kuroshio/Oyashio current system using eddy-resolving models of the North Pacific Ocean. *J. Geophys. Res.*, **101**, 941–976.

Ide, K., P. Courtier, M. Ghil, and A. Lorenc, 1997: Unified notation for data assimilation: operational, sequential and variational. *J. Meteor. Soc. Jpn.*, **75**, 181–189.

Ide, K., L. Kuznetsov, and C. Jones, 2002: Lagrangian data assimilation for point vortex systems. *J. Turbul.*, **3**, 053.

Ikeda, M., 1989: Snow cover detected by diurnal warming of sea ice/snow surface off Labrador in NOAA imagery. *IEEE Trans. Geosci. Remote Sens.*, **27**, 552–560.

Ishikawa, I. and H. Ishizaki, 2009: Importance of eddy representation for modeling the intermediate salinity minimum in the North Pacific: Comparison between eddy-resolving and eddy-permitting models. *J. Oceanogr.*, **65**, 407–426.

Ishikawa, Y., T. Awaji, T. Toyoda, T. In, K. Nishina, T. Nakayama, and S. Shima, 2009: High-resolution synthetic monitoring by a 4-dimensional variational data assimilation system in the northwestern North Pacific. *J. Mar. Syst.*, **78**, 237–248.

Ishizaki, H. and T. Motoi, 1999: Reevaluation of the takano-onishi scheme for momentum advection on bottom relief in ocean models. *J. Atmos. Oceanic Technol.*, **16**, 1994–2010.

Johannessen, J. A., B. Chapron, F. Collard, V. Kudryavtsev, A. Mouche, D. Akimov, and K.-F. Dagestad, 2008: Direct ocean surface velocity measurements from space: Improved quantitative interpretation of Envisat ASAR observations. *Geophys. Res. Lett.*, **35**, L22 608, doi:10.1029/2008GL035709.

Kalnay, E., et al., 1996: The NCEP/NCAR 40-year Re-analysis Project. *Bull. Amer. Meteor. Soc.*, **77**, 437–471.

Kamachi, M. and J. O'Brien, 1995: Continuous data assimilation of drifting buoy trajectory into an equatorial Pacific Ocean model. *J. Mar. Syst.*, **6**, 159–178.

Kawamura, H., K. Mizuno, and Y. Toba, 1986: Formation process of a warm-core ring in the Kuroshio-Oyashio frontal zone–December 1982-October 1982. *Deep-Sea Res.*, **33**, 1617–1640.

Kelly, K. A., L. Thompson, W. Cheng, and E. J. Metzger, 2007: Evaluation of HYCOM in the Kuroshio Extension region using new metrics. *J. Geophys. Res.*, **112**, C01 004.

Lebedev, K. V., H. Yoshinari, N. A. Maximenko, and P. W. Hacker, 2007: YoM-aHa ' 07: Velocity data assessed from trajectories of Argo floats at parking level and at the sea surface. *IPRC Technical Note*, **4(2)**, 16p.

Leonard, B., 1979: A stable and accurate convective modeling procedure based upon quadratic upstream interpolation. *J. Comput. Methods Appl. Mech. Eng.*, **19**, 59–98.

Leonard, B., M. K. MacVean, and A. P. Lock, 1993: Positivity-preserving numerical schemes for multidimensional advection. *NASA Tech. Memo.*, **62**, ICOMP–93–05.

Lin, X. H., L.-Y. Oey, and D.-P. Wang, 2007: Altimetry and drifter data assimilations of loop current and eddies. *J. Geophys. Res.*, **112**, C05 046, doi:10.1029/2006JC003779.

Lorenc, A. C., 1981: A global three-dimensional multivariate statistical interpolation scheme. *Mon. Weather Rev.*, **109**, 701–721.

Masuda, S., T. Awaji, N. Sugiura, Y. Ishikawa, K. Baba, K. Horiuchi, and N. Komori, 2003: Improved estimates of the dynamical state of the North Pacific Ocean from a 4 dimensional variational data assimilation. *Geophys. Res. Lett.*, **30**, 1868.

Masuda, S., T. Awaji, N. Sugiura, T. Toyoda, Y. Ishikawa, and K. Horiuchi, 2006: Interannual variability of temperature inversions in the subarctic North Pacific. *Geophys. Res. Lett.*, **33**, L24 610.

Matthews, J., 2005: Stereo observation of lakes and coastal zones using ASTER imagery. *Remote Sens. Environ.*, **99**, 16–30.

Matthews, J. and T. Awaji, 2010: Synoptic mapping of internal-wave motions and surface currents near the Lombok Strait using the Along-Track Stereo Sun Glitter technique. *Remote Sens. Environ.*, **114**, 1765–1776.

Mitsudera, H., B. Taguchi, Y. Yoshikawa, H. Nakamura, T. Waseda, and T. Qu, 2004: Numerical study on the Oyashio water pathways in the Kuroshio-Oyashio confluence. *J. Phys. Oceanogr.*, **34**, 1174–1196.

Moore, A. M., et al., 2011: The regional ocean modeling system (roms) 4-dimensional variational data assimilation systems part ii - performance and application to the california current system. *Prog Oceanogr*, **91**, 50–73.

Nakamura, T., T. Toyoda, Y. Ishikawa, and T. Awaji, 2006: Effects of tidal mixing at the Kuril Straits on the North Pacific Ventilation: Adjustment of the Intermediate Layer Revealed from Numerical Experiments. *J. Geophys.*

Res., **111**, C04 003, doi: 10.1029/2005JC003142.

Niiler, P. P., N. Maximenko, G. Panteleev, T. Yamagata, and D. Olson, 2003: Nearsurface dynamical structure of the Kuroshio Extension. *J. Geophys. Res.*, **108**, (C3), 3193, doi:10.1029/2002JC001461.

Niiler, P. P., A. L. Sybrandy, K. Bi, P. Poulain, and D. Bitterman, 1995: Measurements of the water-following capability of holey-sock and TRISTAR drifters. *Deep-Sea Res.*, **42**, 1951–1964.

Nodet, M., 2006: Variational assimilation of Lagrangian data in oceanography. *INVERSE PROBLEMS*, **22**, 245–263.

Noh, Y., 2005: Sensitivity to wave breaking and the prandtl number in the ocean mixed layer model and its dependence on latitude. *Geophys. Res. Lett.*, **31**, L23 305.

Noh, Y. and H. J. Kim, 1999: Simulations of temperature and turbulence structure of the oceanic boundary layer with the improved near-surface process. *J. Geophys. Res.*, **104**, 15 621–16 534.

Oey, L. Y. and P. Chen, 1992: A nested -gris ocean model- with application to the simulation of meanders and eddies in the norwegian coastal current. *J. Goephys. Res.*, **97**, 20 063–20 086.

Pazan, S. and P. P. Niiler, 2001: Recovery of near surface velocity from undrogued drifters. *J. Atmos. Oceanic Technol.*, **18**, 476–489.

Qiu, B. and S. Chen, 2005: Variability of the Kuroshio Extension jet, recirculation gyre and mesoscale eddies on decadal timescales. *J. Phys. Oceanogr.*, **35**, 2090–2103.

Qiu, B., S. Chen, and P. Hacker, 2007: Effect of Mesoscale Eddies on Subtropical Mode Water Variability from the Kuroshio Extension System Study (KESS). *J. Phys. Oceanogr.*, **37**, 982–1000.

Rio, M. H. and F. Hernandez, 2004: A mean dynamic topography computed over the world ocean from altimetry, in situ measurements, and a geoid model. *J. Geophys. Res.*, **109**, C12 032.

Romeiser, R., J. Johannessen, B. Chapron, F. Collard, V. Kudryavtsev, H. Runge, and S. Suchandt, 2010: *Direct Surface Current Field Imaging from Space by Along-Track InSAR and Conventional SAR.* In: V Barale, J. F. R. Gower, L. Alberotanza Oceanography from Space: Revisited, Springer Verlag, Berlin, pp. 73-91.

Romeiser, R. and H. Runge, 2007: Theoretical Evaluation of Several Possible Along-Track InSAR Modes of TerraSAR-X for Ocean Current Measurements. *IEEE Trans. Geosci. Remote Sens.*, **45**, 21–35.

Roske, F., 2001: An atlas of surface fluxes based on the ECMWF re-analysis – a climatological dataset of force global ocean general circulation models. *Rep.*, **323**, 26pp, Max-Plank Inst. fur Meteor., Hamburg, Germany.

Stammer, D., C. Wunsch, I. Fukumori, and J. Marshall, 2002: State estimation improves prospects for ocean research. *EOS, Trans. Amer. Geophys. Union*, **83**, 289–293.

Sugimoto, T., Y. Kawasaki, and J. Li, 1992: A description of the time-dependent hydrographic structure of the warm streamer around the Kuroshio warm-core ring 86B. *Deep-Sea Res.*, **39**, S77–S96.

Talley, L. D., 2003: Shallow, intermediate, and deep overturning components of the global heat budget. *J. Phys. Oceanogr.*, **33**, 530–560.

Toyoda, T., T. Awaji, Y. Ishikawa, and T. Nakamura, 2004: Preconditioning of Winter Mixed Layer in the Formation of North Pacific Eastern Subtropical Mode Water. *Geophys. Res. Lett.*, **31**, L17 206.

Usui, N., H. Tsujino, Y. Fujii, and M. Kamachi, 2008a: Generation of a trigger meander for the 2004 Kuroshio large meander. *J. Geophys. Res.*, **113**, C01 012, doi:10.1029/2007JC004266.

Usui, N., H. Tsujino, H. Nakano, and Y. Fujii, 2008b: Formation process of the Kuroshio large meander in 2004. *J. Geophys. Res.*, **113**, C08 047, doi:10.1029/2007JC004675.

Yasuda, I., 2003: Hydrographic structure and variability of the Kuroshio-Oyashio Transition Area. *J. Oceanogr.*, **59**, 389–402.

Yu, P., A. L. Kurapov, G. D. Egbert, J. S. Allen, and P. M. Kosro, 2012: Variational assimilation of hf radar surface currents in a coastal ocean model off oregon. *Ocean Modelling*, **49-50**, 86–104.
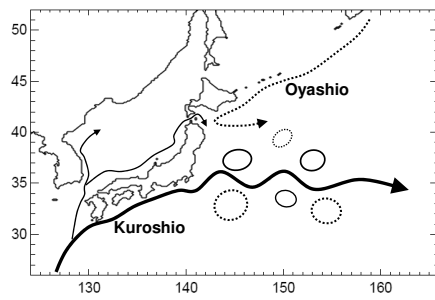
Fig. 1 Schematic view of the circulation field in the northwestern North Pacific. Solid (Dotted) lines denote warm (cold) water currents and eddies
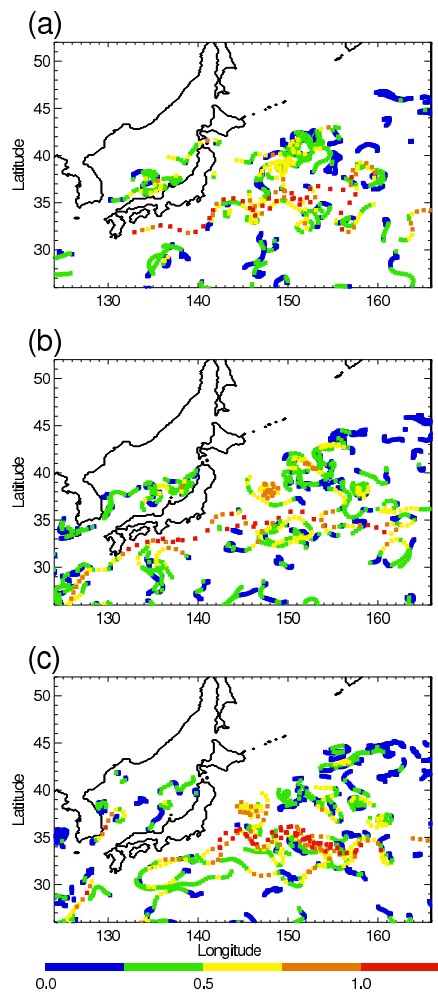
Fig. 2 Distribution of preprocessed daily-averaged velocity data derived from surface drifters in each Period ((a) Period 1, (b) Period 2, (c) Period 3); the colors of the symbols indicate the velocity values shown with bottom color bar
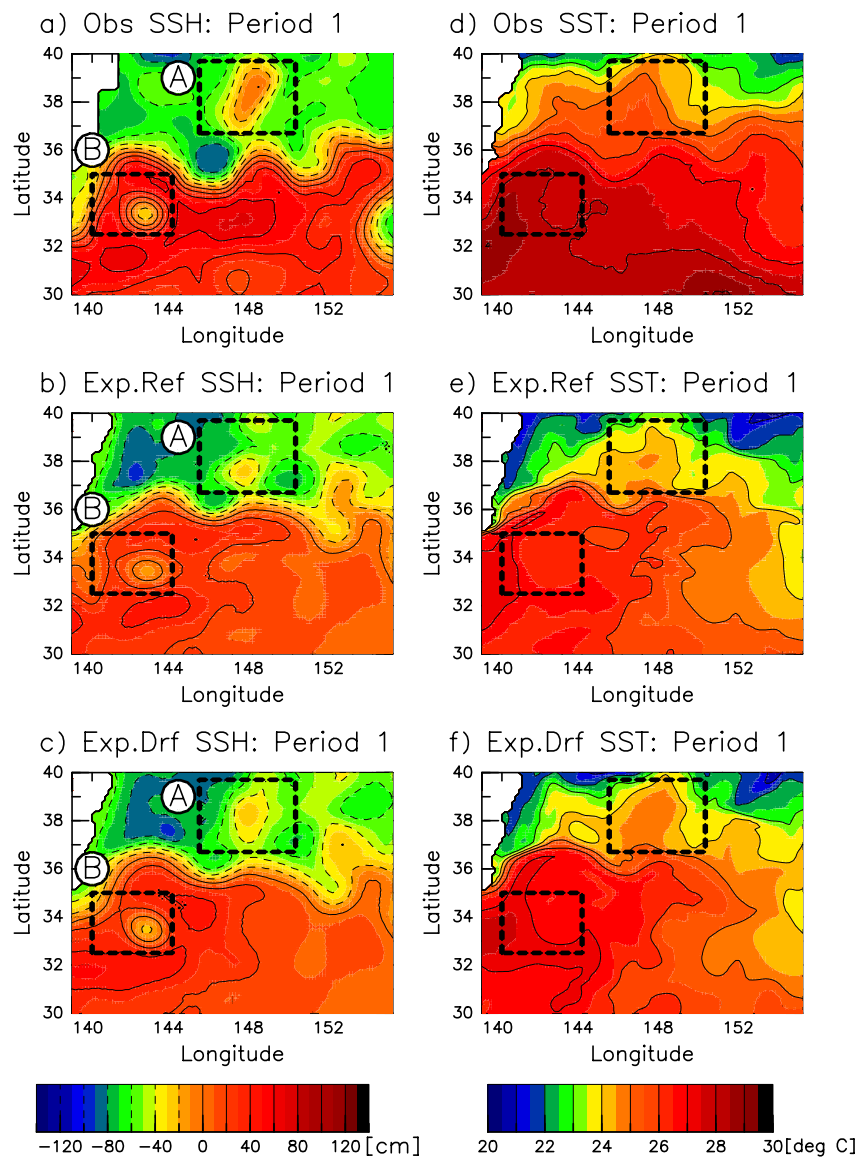
Fig. 3 SSH (left) and SST (right) fields averaged over Period 1; (top) satellite objective map, (middle) Exp. Ref, (bottom) Exp. Drf. Rectangular boxes with dashed black line denote examples of improved meso-scale features
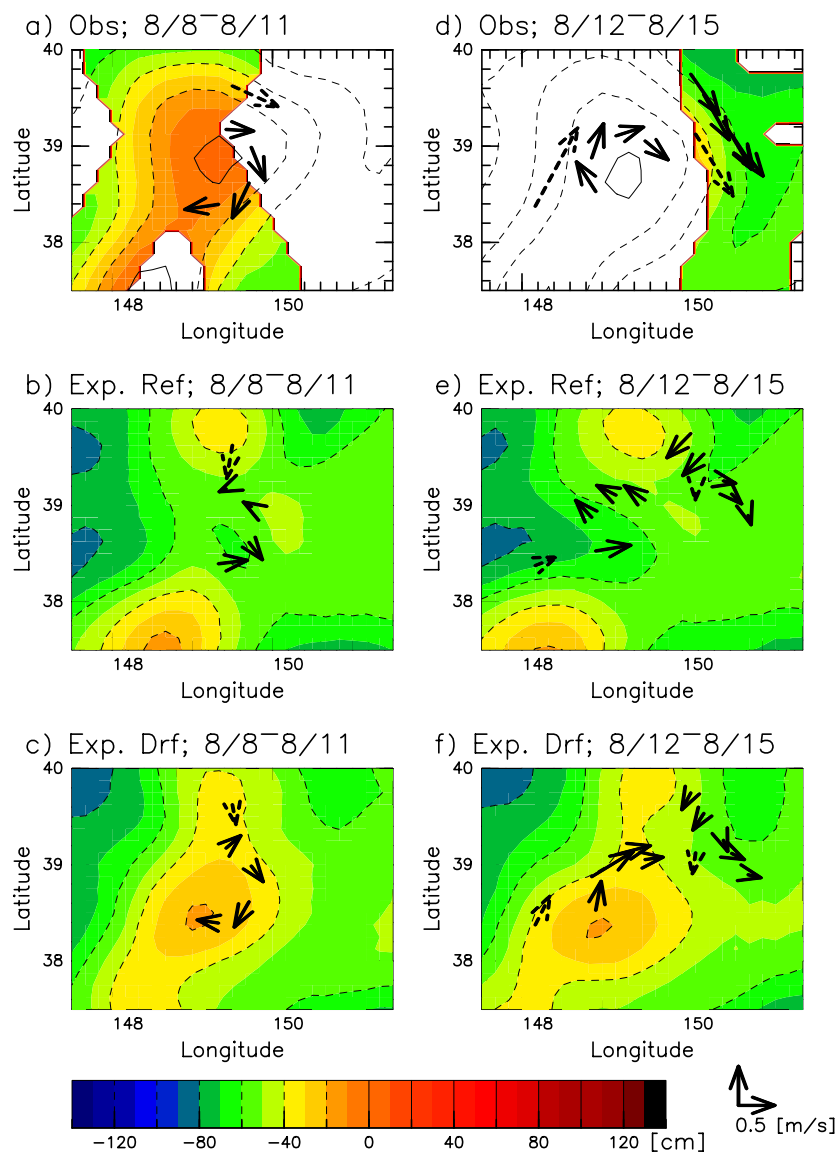
Fig. 4 SSH fields in the region centered at $149°$E, $39°$N for (left) 2005/8/8-11 and (right) 2005/8/12-15; (top) 3.5 daily satellite objective maps, 3.5-day-averaged reproduced SSH maps of (middle) Exp. Ref and (bottom) Exp. Drf. Solid black arrows are surface velocity vectors (top) derived from drifter data and (middle, bottom) picked up from each reproduced circulation field. Dashed black arrows are surface velocity vectors (top) derived from YoMaHa'07 dataset and (middle, bottom) picked up from each reproduced circulation field
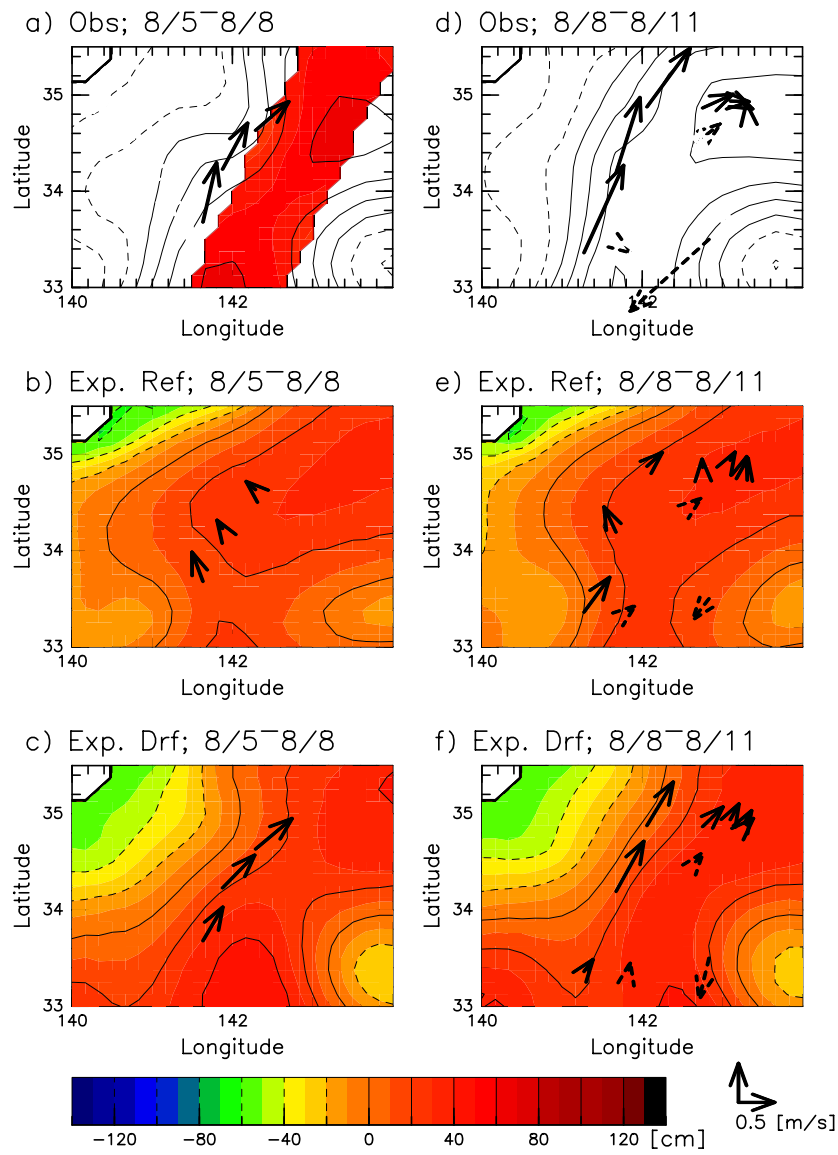
Fig. 5 Same as Figs. 4 but for (left) 2005/8/5-8 and (right) 2005/8/8-11 in the region centered at 142°E, 34°N
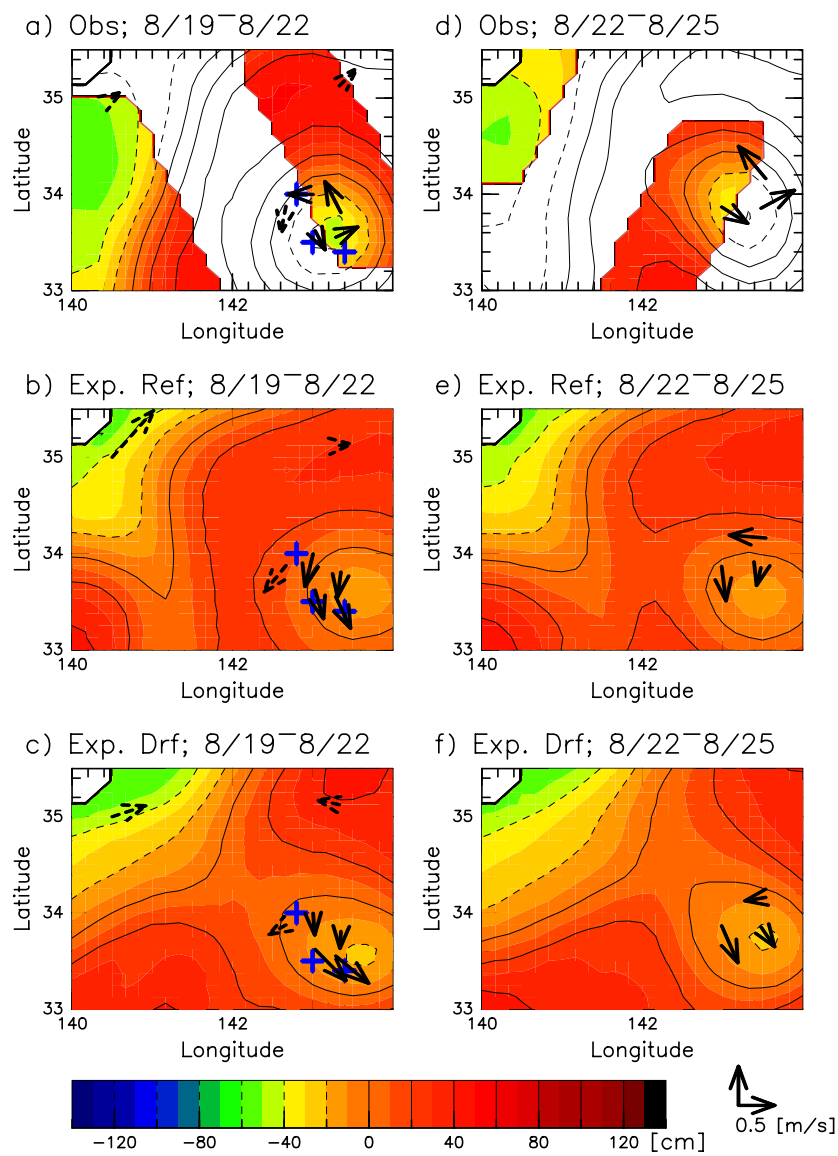
Fig. 6 Same as Figs. 5 but for (left) 2005/8/19-22 and (right) 2005/8/22-25. Blue plus symbols indicate the positions of in-situ observations
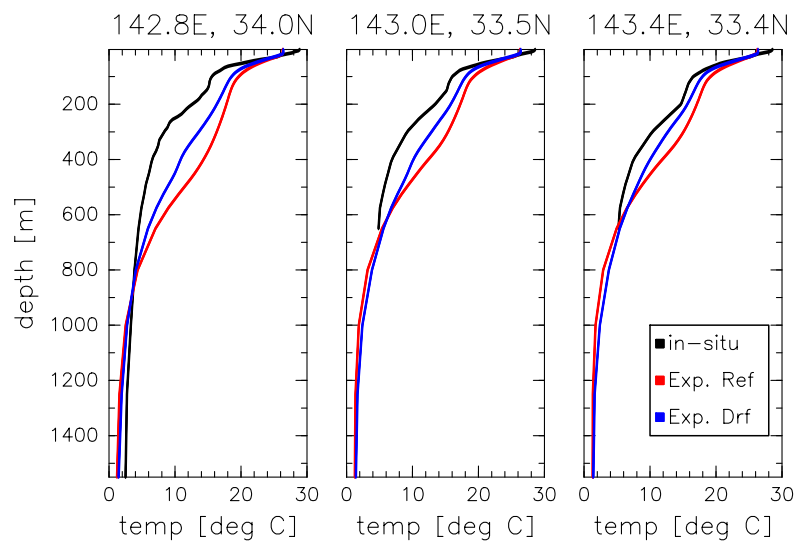
Fig. 7 In-situ temperature profiles (black line) shown in Figs. 6, with corresponding reproduced temperature profiles (red: Exp. Ref, blue: Exp. Drf)
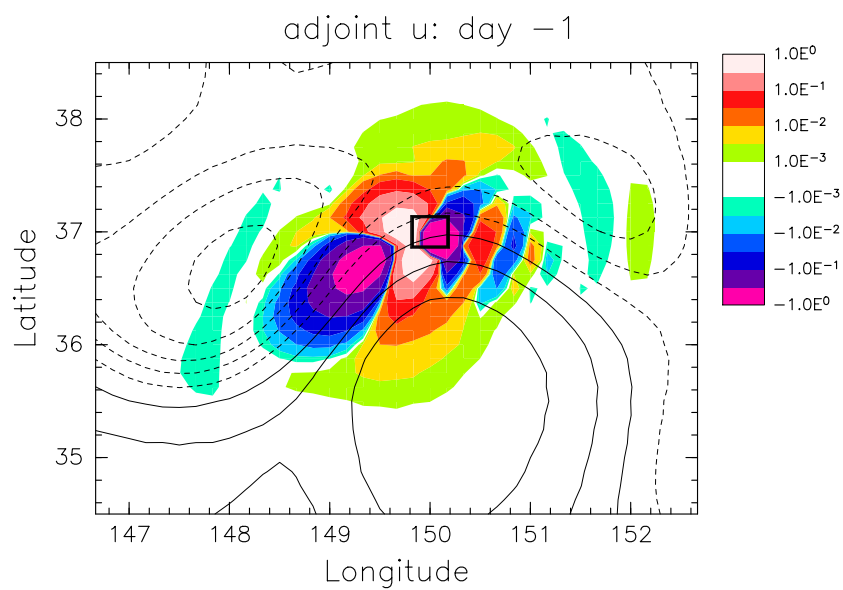

Fig. 8 Adjoint zonal velocity field at the top layer on day −1 near the input region. Tone shows values of adjoint zonal velocity. Contour lines show the SSH at 20 cm intervals (solid lines denote positive values, dashed lines denote negative values). Rectangular boxes with solid black lines denote the region in which the initial input signal was provided
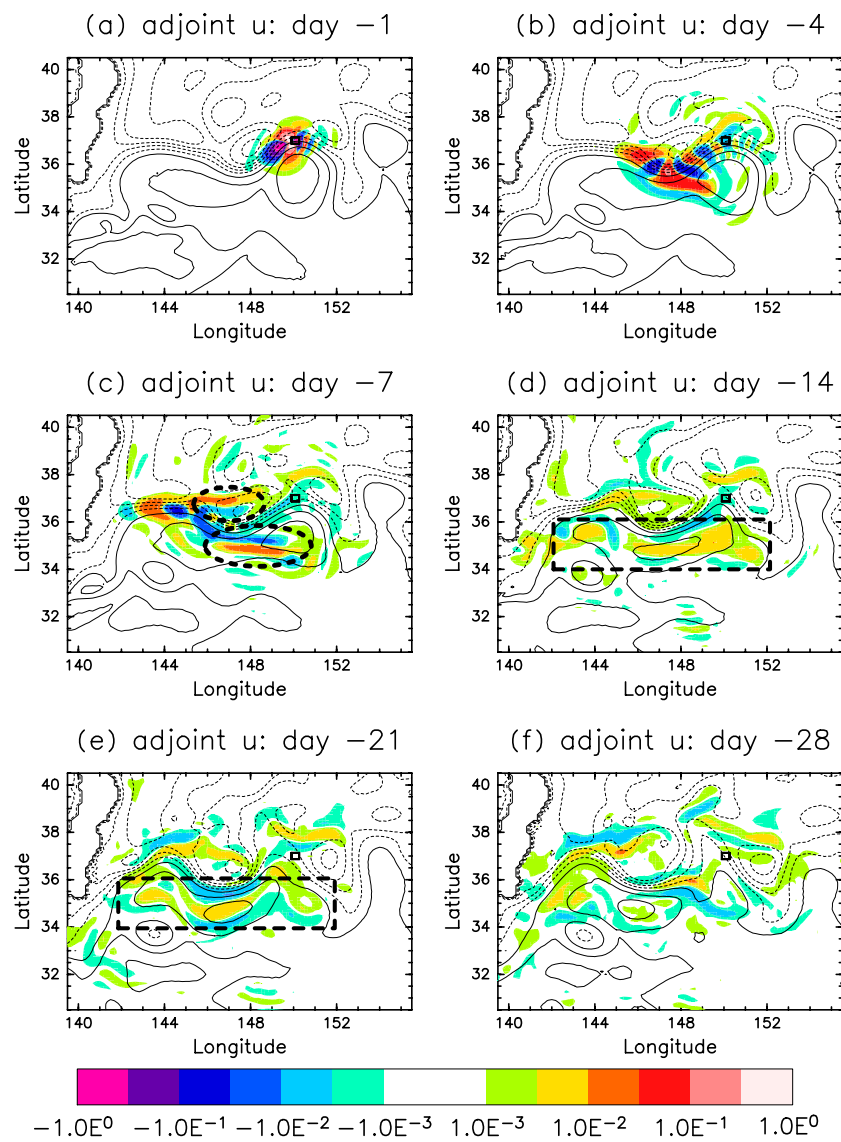
Fig. 9 Same as Fig. 8a for KE region and time series. Circles and boxes with dashed black line are explained in the main text
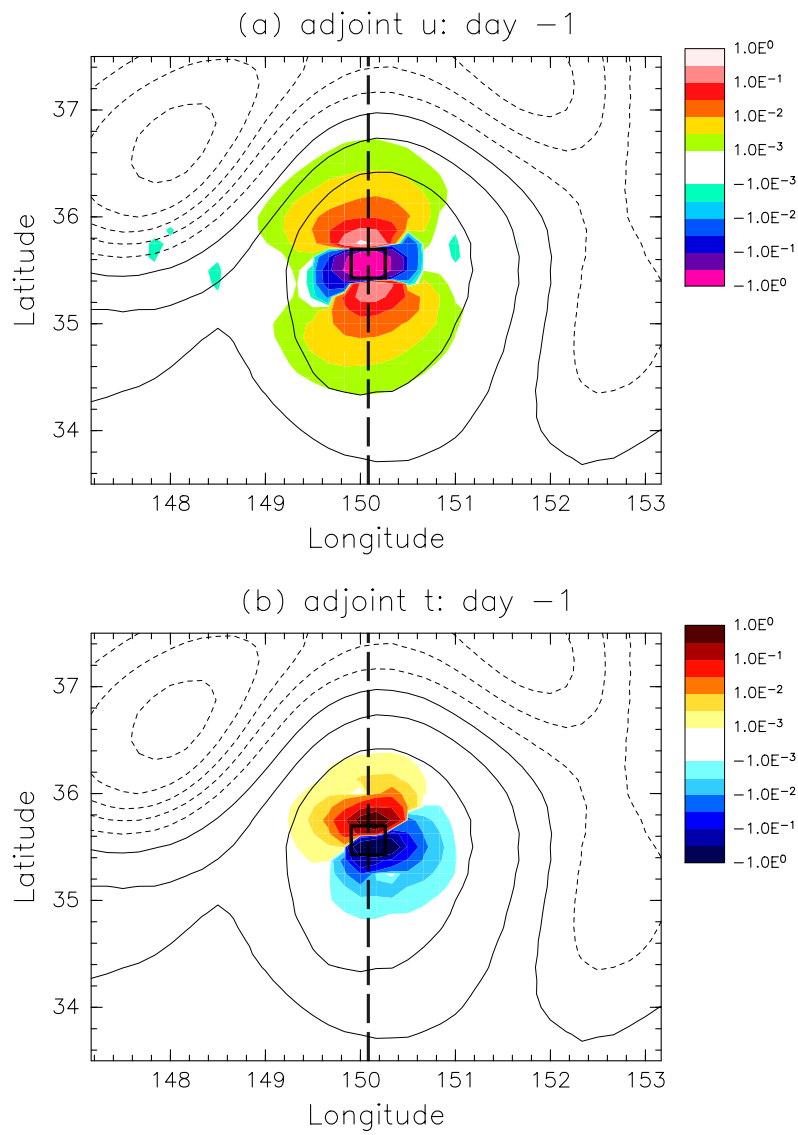
Fig. 10 Same as Fig. 8 but for the additional adjoint sensitivity experiment, (top) adjoint zonal velocity field at the top layer and (bottom) adjoint temperature field at the top layer. Dashed black lines indicate the locations of the meridional sections shown in Figs. 11
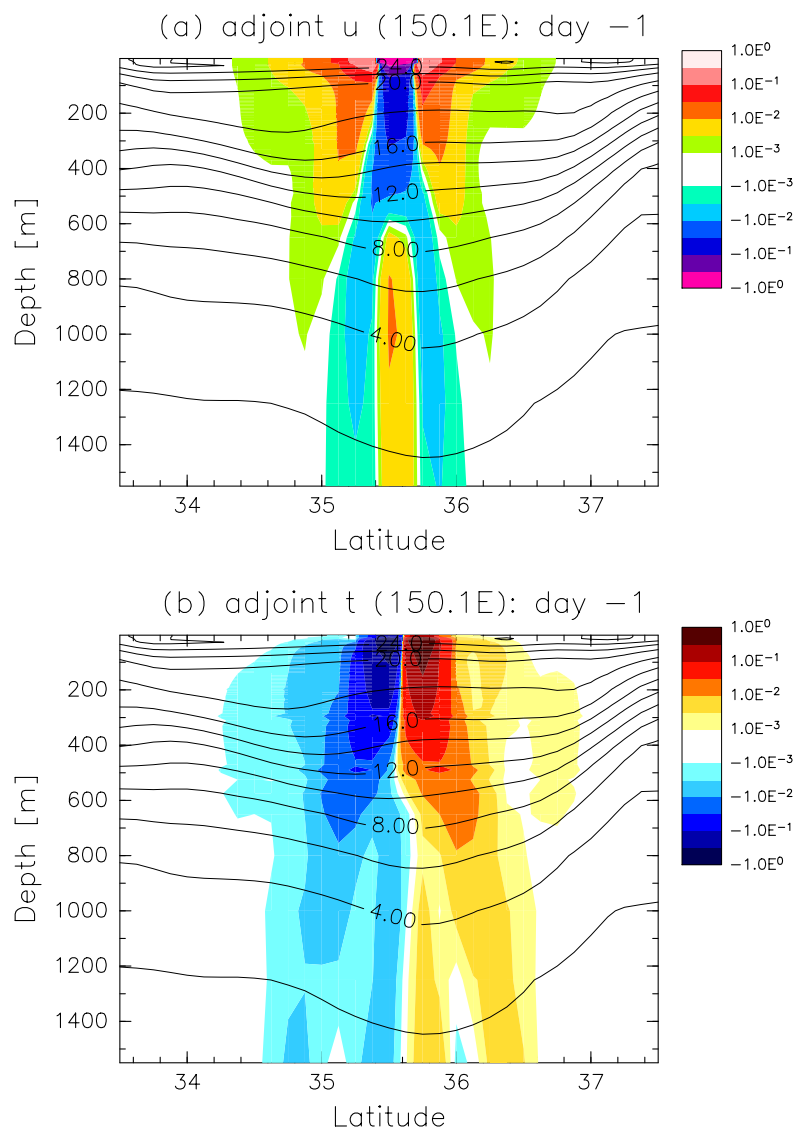
Fig. 11 Same as Fig. 10 but for the meridional section with background temperature field along the dashed line in Figs. 10.

Table 1 The "Improvement rate" for each component in each Period; RMSD values are spatially averaged in the KE region

	Period 1	Period 2	Period 3
Drifter	16.1%	11.6%	6.5%
SST	8.4%	8.2%	-10.1%
SSH	6.8%	5.9%	-2.7%
T Prof	21.2%	17.8%	-20.8%
S Prof	14.4%	11.8%	-12.1%
YoMaHa	7.4%	2.4%	-1.9%